 ICCES, vol.9, no.2, pp.81-93

Nanojet Vaporization Analysis by Molecular Dynamics Simulation

Chun-Lang Yeh[1]

Summary

In this study, the vaporization process of a nanojet is investigated by molecular dynamics simulation. Liquid argon nanojet made of 44000 Lennard-Jones molecules is investigated under various simulation parameters to examine their influence on the nanojet vaporization process. Snapshots of the molecules, evolution of the density field, and evolution of the intermolecular force are analyzed. The present simulation results can provide insight into the fundamental mechanism of the atomization process and will be helpful for the design of nanojet devices such as nano-printer or nano-sprayer.

keywords: Nanojet, Vaporization Process, Molecular Dynamics Simulation

Nomenclature

F	intermolecular force
k_B	Boltzmann constant
L	fundamental cell characteristic length
m	molecular mass
N	number of molecules
r	intermolecular distance
r_c	cut-off radius of Lennard-Jones potential function
T	temperature
t	time
Δt	time step
V	volume
v_i	velocity of molecule i
x, y, z	Cartesian coordinates

Greek

ε	energy parameter of Lennard-Jones potential function
ρ	density
σ	length parameter of Lennard-Jones potential function
ϕ	Lennard-Jones potential function

Subscripts

[1]Department of Aeronautical Engineering, National Formosa University, Huwei, Yunlin 632, Taiwan, R.O.C., Tel: G886-5-6315527, Fax: 886-5-6312415, Email: clyeh@nfu.edu.tw

L liquid phase
V vapor phase

Superscripts

* non-dimensionalized quantity
_ averaged quantity

Introduction

Recently, the evolution of a nanojet has received considerable attentions due to its unique characteristics and wide range of applications, e.g. ink-jet printing, fuel injection, bioengineering, etc. Previous theories and modeling techniques about jet injection have been developed focused on much larger thermodynamic systems with continuum assumptions. However, direct application of these theories to nano-scale systems is uncertain. Conventional liquid jet breakup and spray models require many assumptions and experimental correlations that are difficult to obtain in nanojet. Nanojet devices use an actuator to eject atoms or molecules through a nano-nozzle. However, the fabrication of the actuator and nano-nozzle is very complex. In addition, there exist major challenges for the nano-locating and nano-driving systems and assembly of these components. Therefore, to build a nanojet actually is still a complex task. On the other hand, molecular dynamics (MD) can offer novel insights into the underlying atomistic mechanisms and nanometer-scale behavior due to their high temporal and spatial resolution.

In Fig.1, the fluid/air interface for atomizer flow by macroscopic analysis from one of the author's previous studies [1] is shown. It can be seen that the liquid evolves into threads in motion after leaving the atomizer. In the author's another previous study [2], the vaporization process of a nano-scale liquid thread in vapor or vacuum is analyzed by MD. The formation of liquid threads, like nanojet, is one of the most fundamental and important phenomena during the atomization process. The analysis focuses not only on the liquid particle formation but also on its subsequent evolution, which involves breakup, collision, and coalescence of the liquid particles. These phenomena play important roles in the entire vaporization process. From the study, it is also found that Rayleigh's stability criterion [3] holds down to the molecular scale. Similar results have also been reported by Koplik and Banavar [4], as well as Kawano [5]. However, the above simulation models are limited to an initially quiescent liquid thread, which is not emanating but intrinsically rearranges itself into droplets or smaller liquid threads. In addition, the MD simulation results of a time-dependent liquid flow are sensitive to initial velocities. Therefore, the above results can not be generalized to nanojets.

Moseler and Landman [6] reported MD simulation results for the formation and instability of liquid nanojet. They pointed out that the details of nanojet breakup

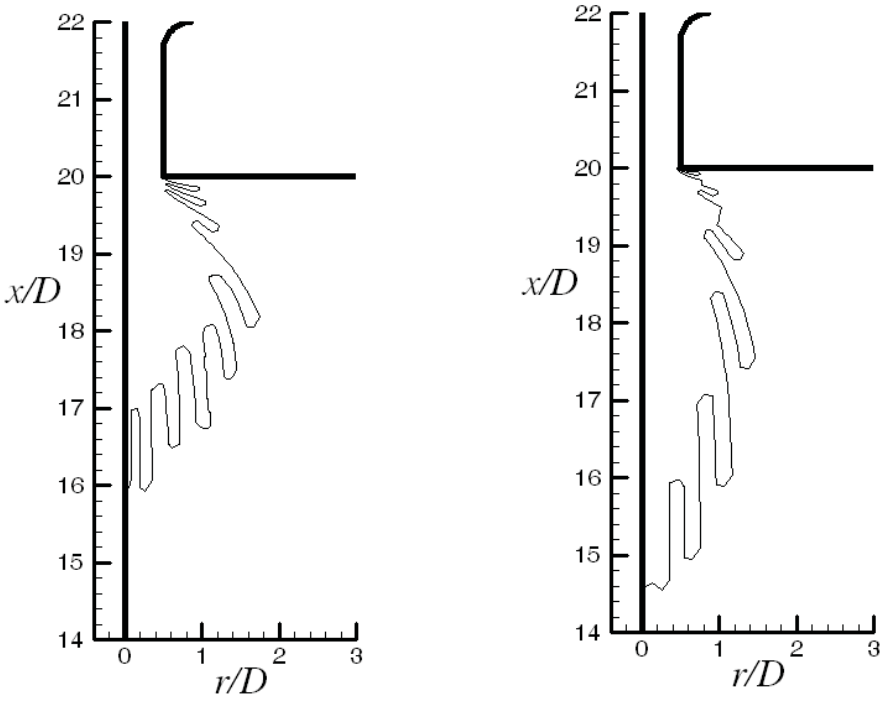

(a) by standard k-ε model (b) by Gatski-Speziale's ARSM model

Figure 1: Fluid/air interface for atomizer flow by macroscopic analysis [1]

behavior obtained by MD are significantly different from the Navier-Stokes result. Shin et al. [7] simulated argon nanojet injection under vacuum conditions by MD. They found that different injector shapes does not cause significant change in the nanojet breakup behavior. On the other hand, the liquid temperature inside the injector was found to be a controlling factor for the subsequent breakup characteristics. A higher liquid temperature is preferred for a faster nanojet breakup with a shorter breakup length. Choi et al. [8] investigated the capillary instability of nanometer-sized surface-tension-driven flow by MD with Lennard-Jones fluid. They found that the thermal fluctuation, which is significant in a nano-scale system, is the most important factor for various breakup scenarios of a nanojet.

In this study, liquid argon nanojets made of 44000 Lennard-Jones molecules are investigated under various simulation parameters to examine their influence on the nanojet vaporization process. This will be helpful for the design of nanojet devices such as nano-printer or nano-sprayer and can provide insight into the fundamental mechanism of the atomization process.

Molecular Dynamics Simulation Method

In this study, the vaporization process of a liquid argon nanojet discharged into vacuum is investigated by molecular dynamics (MD) simulation. The inter-atomic potential is one of the most important parts of MD simulation. Many possible potential models exist, such as hard sphere, soft sphere, square well, etc [9]. In this research, the Lennard-Jones 12-6 potential model, which is widely used, is adopted for calculation. It is

$$\phi(\mathrm{r}) = 4\varepsilon\left[\left(\frac{\sigma}{r}\right)^{12} - \left(\frac{\sigma}{r}\right)^{6}\right] \tag{1}$$

where r denotes the distance between two molecules, ε and σ are the representative scales of energy and length, respectively. The Lennard-Jones fluid in this research is taken to be argon for its ease of physical understanding. The parameters for argon are as follows [5] : the length parameter σ=0.354 nm, the energy parameter ε/k_B=93.3K, and the molecular weight $m = 6.64 \times 10^{-26}$ kg, where $k_B = 1.38 \times 10^{-23}$ J/K denotes the Boltzmann constant. The cut-off radius r_c beyond which the intermolecular interaction is neglected is 5.0σ.

Table 1: Nano-nozzle dimensions, temperatures, number of molecules and simulation results

Case	L_2^*	L_3^*	L_4^*	L_5^*	$D^*/2$	T_D^*	N	$\overline{f_\rho}$
1	5.73	5.73	5.73	76.7	8.81	0.75	43970	1.34
2	5.73	5.73	5.73	76.7	8.81	1.5	43970	1.08
3	5.73	5.73	5.73	76.7	8.81	2.0	43970	0.94
4	5.73	5.73	5.73	76.7	8.81	3.0	43970	0.74
5	5.73	5.73	5.73	76.7	8.81	4.5	43970	0.59
6	8.66	5.73	2.79	76.7	8.81	2.0	43989	0.95
7	2.79	5.73	8.66	76.7	8.81	2.0	43949	0.92
8	5.73	8.67	5.73	76.7	5.87	2.0	43934	1.27

The nano-nozzle is schematically shown in Fig.2. The simulation domain comprises a cubical box of side length 3600, with periodic boundary conditions applied in all three directions. The nano-nozzle is placed at the center of the box. Simulation parameters are listed in Table 1, which include nano-nozzle dimensions, temperatures, number of molecules and simulation results. The time integration of motion is performed by Gear's fifth predictor-corrector method [9] with a time step of μt^*=0.0001 (i.e. 0.25 fs). The initial number density of the liquid argon within the nano-nozzle is ρ_L^*=0.819. Note that all quantities with an asterisk in this paper, such as L^*, D^*, ρ^*, μt^*, T^*, etc., are non-dimensionalized in terms of σ, ε, and m, i.e. $L^* = L/\sigma$, $D^* = D/\sigma$, $\rho^* = N\sigma^3/V$, $\mu t^* = \mu t(\varepsilon/m)^{1/2}/\sigma$, $T^* = k_B T/\varepsilon$.

The argon atoms inside the nano-nozzle are liquid and the nano-nozzle is made of rigid argon atoms. A push panel composed of 600 argon atoms is constructed

with a downward velocity of 120m/s. In this study, the interactions among liquid argon atoms, nano-nozzle and push panel are taken into account.

Velocity rescaling is performed at each time step by the following correction to make sure that the system is at the desired temperature :

$$v_i^{new} = v_i^{old} \sqrt{\frac{T_D}{T_A}} \tag{2}$$

where v_i^{new} and v_i^{old} are the velocities of molecule i after and before correction, respectively, and T_D and T_A are the desired and the actual system temperatures, respectively. A minimum image method and the Verlet neighbor list scheme [9] to keep track of which molecules are actually interacting at a given time interval of 0.005 are used.

Results and Discussions

In the following discussion, a liquid argon nanojet of length L_5^* and diameter $2L_3^* + D^*$ is pushed by a panel into vacuum through a nano-nozzle of orifice diameter D^*, as illustrated in Fig.2. Simulation conditions are listed in Table 1.

Nanojet Vaporization Process

Figure 3 shows the snapshot of a nanojet at $t^* = 80$ with the conditions of $L_2^* = L_3^* = L_4^* = 5.73$, L_5^*=76.7, $D^*/2$=8.81 and T^*=0.75, which corresponds to a nanojet of length 26.2 nm and diameter 10 nm, and a nano-nozzle of orifice length 2nm, diameter 6 nm, as well as an actual temperature of 70 K. The dot in Fig.3 indicates the center of the molecule. From the figure it is found that the nanojet does not break up. Owing to the low temperature, the molecular kinetic energies are so low that the molecules congregate near the orifice exit. Very few liquid molecules are evaporated at this low temperature. At a higher temperature T^*=1.5 (140 K), as shown in Fig.4, the molecules leave the orifice exit earlier than at T^*=0.75, due to their higher molecular kinetic energies. More liquid molecules are evaporated at this higher temperature. However, like at T^*=0.75, the nanojet has not broken up before t^*=80. If the temperature is further increased to T^*=2.0 (187 K), as shown in Fig.5, evident evaporation is observed. Many evaporated molecules are produced and the non-evaporated liquid molecules concentrate within the central region. Figure 6 shows the snapshots for temperature T^*=3.0 (278 K). It is observed that breakup of the nanojet occurs and its spray angle is larger than at T^*=2.0. The spurted molecules from the nano-nozzle are more evenly distributed at this temperature. If the temperature is further increased to T^*=4.5 (420 K), as shown in Fig.7, the spray angle is even larger than at T^*=3.0 and the spurted molecules from the nano-nozzle are much more uniformly distributed as compared to the lower temperature cases. Comparison of Figs.3, 4, 5, 6 and 7 reveals that the liquid nanojet evaporates quicker at higher temperatures. This will be further illustrated

in later sections discussing the density distribution and the intermolecular force.

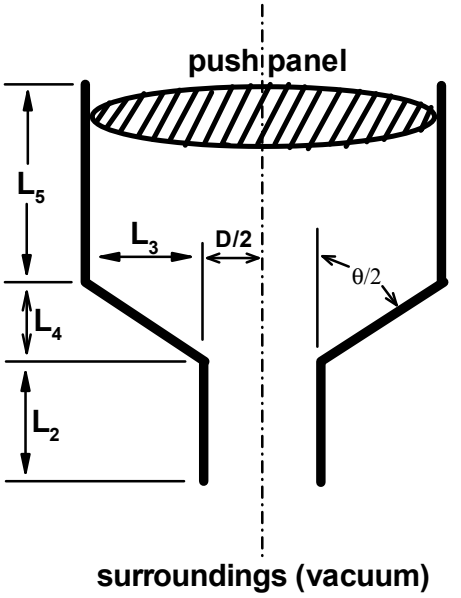

Figure 2: Illustration of the nano-nozzle configuration and dimensions

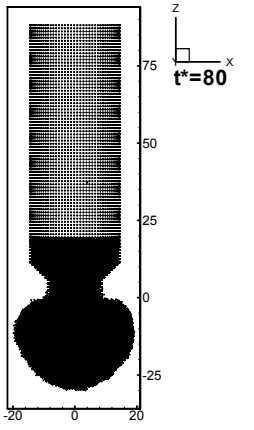

Figure 3: Snapshot at t^*=80 for case 1 in Table 1 (L_2^* =5.73, L_3^* =5.73, L_4^* =5.73, L_5^* =76.7, $D^*/2$=8.81, T_D^*=0.75)

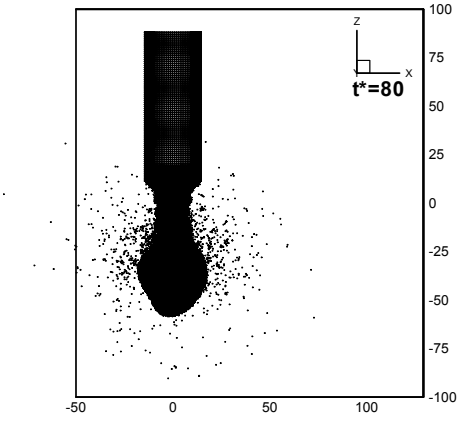

Figure 4: Snapshot at t^*=80 for case 2 in Table 1 (L_2^* =5.73, L_3^* =5.73, L_4^* =5.73, L_5^* =76.7, $D^*/2$=8.81, T_D^*=1.5)

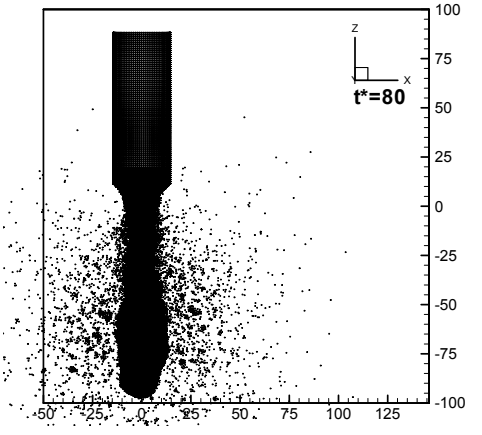

Figure 5: Snapshot at t^*=80 for case 3 in Table 1 (L_2^* =5.73, L_3^* =5.73, L_4^* =5.73, L_5^* =76.7, $D^*/2$=8.81, T_D^*=2.0)

To investigate the influence of the nozzle geometry on nanojet vaporization, comparison of the snapshots at t^*=80 and T^*=2.0 for four different nozzle geome-

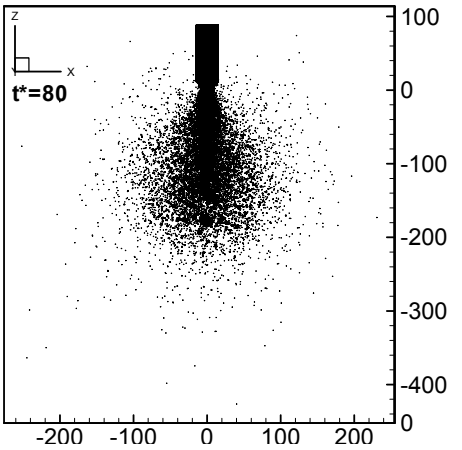

Figure 6: Snapshot at t^*=80 for case 4 in Table 1 (L_2^* =5.73, L_3^* =5.73, L_4^* =5.73, L_5^* =76.7, $D^*/2$=8.81, T_D^*=3.0)

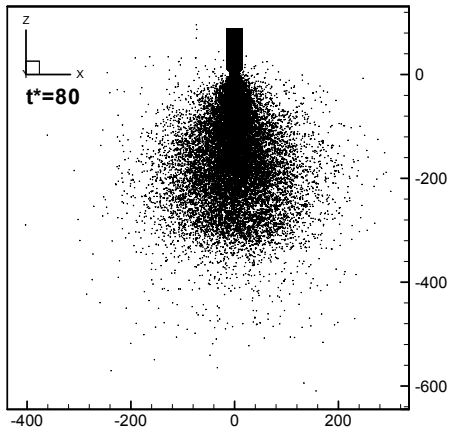

Figure 7: Snapshot at t^*=80 for case 5 in Table 1 (L_2^* =5.73, L_3^* =5.73, L_4^* =5.73, L_5^* =76.7, $D^*/2$=8.81, T_D^*=4.5)

tries is shown in Fig.8. Note that Figs.8(a), (b), (c) and (d) correspond to cases 6, 3, 7 and 8, respectively, in Table 1. In Figs.8(a), (b) and (c), the nozzle orifice diameters are equal (6 nm) but the nozzle orifice lengths are varied; while in Fig.8(d), the nozzle orifice length is the same as for Fig.8(b) (2 nm) but the nozzle orifice diameter is smaller (4 nm). It can be observed by a careful comparison of Figs.8(a), (b) and (c) that, on the basis of identical nozzle orifice diameter, a nanojet from a nozzle with a shorter orifice length (L_2) moves farther. On the other hand, from Figs.8(b) and (d), on the basis of identical nozzle orifice length, a nanojet from a nozzle with a larger orifice diameter moves farther. As pointed out by Lefebvre [10], in a practical plain-orifice atomizer, frictional loss increases with nozzle orifice length/diameter ratio. Therefore, a nanojet from a nozzle with a smaller orifice length/diameter ratio moves farther due to its smaller frictional loss. This will be further illustrated in later sections discussing the density distribution and the intermolecular force.

Density Distribution

It is important that the system be in equilibrium state before statistical values of the local properties can be taken. However, owing to the computational capacity limitations, the MD simulation can not proceed to a macroscopically long period. Nevertheless, the purpose of this paper is not to discuss statistical values of the local properties but to investigate the vaporization process of a nanojet, which is important and conducive to the understanding of the fundamental mechanism of the atomization process. Criteria have to be made to quantify the discussion regard-

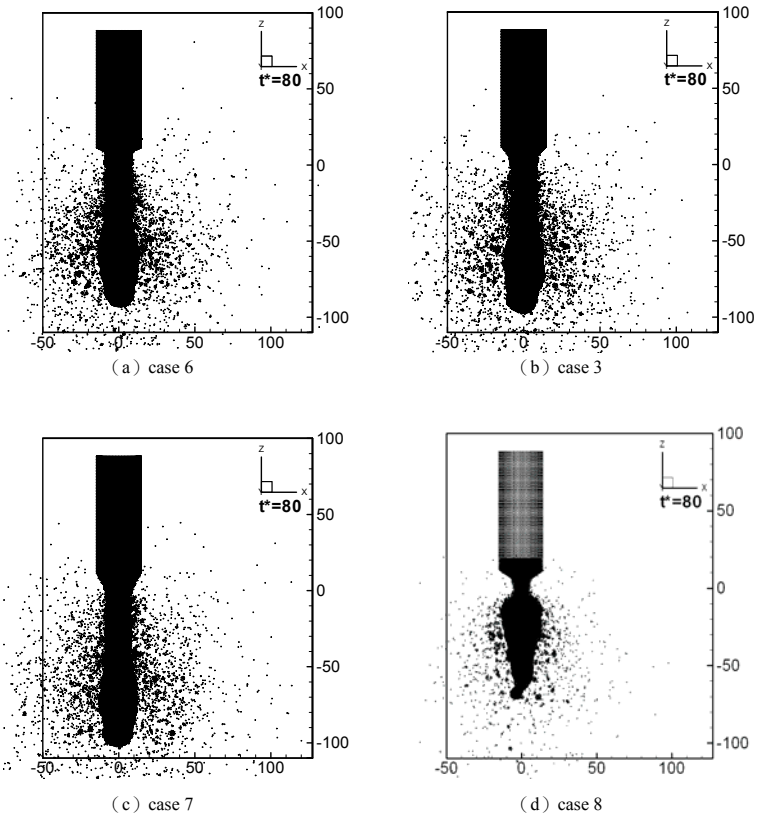

(a) case 6 (b) case 3

(c) case 7 (d) case 8

Figure 8: Comparison of the snapshots at t^*=80 and T^*=2.0 for four different nozzle geometries

ing the nanojet vaporization process. Unfortunately, such criteria are still arbitrary in the literature. Because the system temperature in this study is kept at the desired temperature, a constant temperature criterion is not suitable for the discussion of the vaporization process. In this research, a nanojet is considered to vaporize faster if the distribution of molecules reaches a uniform state quicker during the vaporization process. This criterion essentially concerns with the evolution of the density distribution. The density at a specified point in the fundamental cell can be defined as

$$\rho = \lim_{\delta V \to 0} \frac{\delta N}{\delta V} \tag{3}$$

where δV is a small volume surrounding the point considered and δN is the number of molecules inside the volume δV. The density defined by Eq.(3) is actually an averaged density of a small volume surrounding the point considered. The value will approach the density of a specified point if the volume δV shrinks to that point. However, for a meaningful density field, the volume δV can not be

too small because when δV becomes too small, it is difficult to obtain a definite value for $\delta N/\delta V$. In this study, the volume δV is taken to be a sphere with non-dimensionalized radius R^*=2 and with its center located at the point considered. This is an optimal choice after numerical test.

Figure 9 shows the evolution of density uniformity factor for nanojets at different temperatures (cases 1∼5 in Table 1) and the conditions of $L_2^* = L_3^* = L_4^*$=5.73, L_5^*=76.7, D^*/2=8.81. The density uniformity factor is defined as

$$f_\rho = \frac{\sum_N \left(\rho^* - \rho_{eq}^*\right)_{t^*} \Delta V}{\sum_N \left(\rho^* - \rho_{eq}^*\right)_{t^*=0} \Delta V} \tag{4}$$

where N is the initial number of liquid molecules in the fundamental cell, ρ^* and V are the density and volume of molecule i, respectively, as defined by Eq.(3), and ρ_{eq}^* is the density value when the molecules are uniformly distributed, i.e. $\rho_{eq}^* \equiv N/$ Vol, where Vol is the volume of the fundamental cell. The density uniformity factor f_ρ as defined by Eq.(4) represents the deviation from uniform state. From Fig.9 it is observed that a higher temperature nanojet evaporates faster than a lower temperature one and this corroborates the results of Figs.3∼7 as discussed in section 3.1. The time averaged value of the density uniformity factor, $\overline{f_\rho}$, in a time interval of t^*=0 to 80, as listed in Table 1, also reveals this observation. In Fig.9, it is noted that at lower temperatures (T^*=0.75 and 1.5), the density uniformity factor increases first and then decreases. For a lower temperature nanojet, the momenta of the liquid molecules away from the push panel in the nano-nozzle are low while the molecules near the push panel have relatively larger momenta. This results in a compression effect and leads to the increase of the density uniformity factor at the earlier stage of the vaporization process. Figure 10 shows the evolution of density uniformity factor for different orifice lengths (cases 3, 6 and 7 in Table 1) on the basis of identical nozzle orifice diameter (6 nm) and the conditions of L_3^*=5.73, L_5^*=76.7, T^*=2.0. It is observed that a nanojet with a shorter orifice length evaporates quicker. This corroborates the results of Figs.8(a), (b) and (c) as discussed in section 3.1 : a nanojet from a nozzle with a smaller orifice length/diameter ratio moves farther due to its smaller frictional loss. Figure 11 shows the evolution of density uniformity factor for different orifice diameters (cases 3 and 8 in Table 1) on the basis of identical nozzle orifice length (2 nm) and the conditions of L_4^*=5.73, L_5^*=76.7, T^*=2.0. It is observed that a nanojet with a larger orifice diameter evaporates quicker. This corroborates the results of Figs.8(a) and (d) and also reveals the above observation that a nanojet from a nozzle with a smaller orifice length/diameter ratio moves farther due to its smaller frictional loss.

Intermolecular Force

The intermolecular force is an indication of the surface tension experienced by

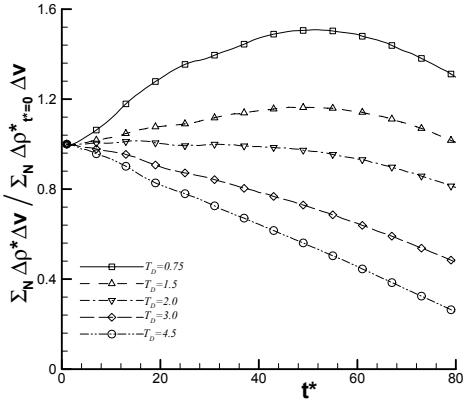

Figure 9: Evolution of the density uniformity factor for different temperatures (cases 1∼5 in Table 1)

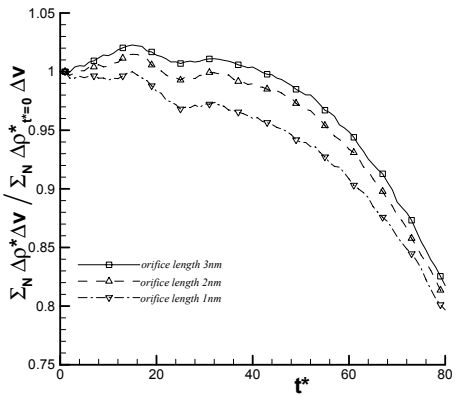

Figure 10: Evolution of the density uniformity factor for different orifice lengths (cases 3, 6 and 7 in Table 1)

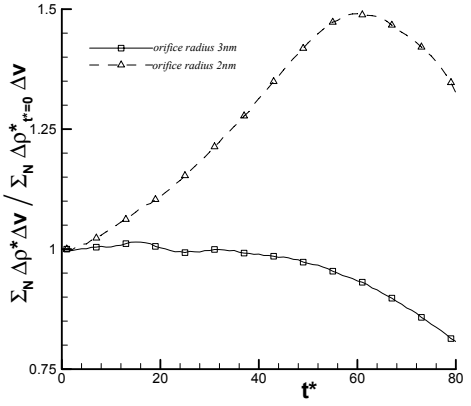

Figure 11: Evolution of the density uniformity factor for different orifice radii (cases 3 and 8 in Table 1)

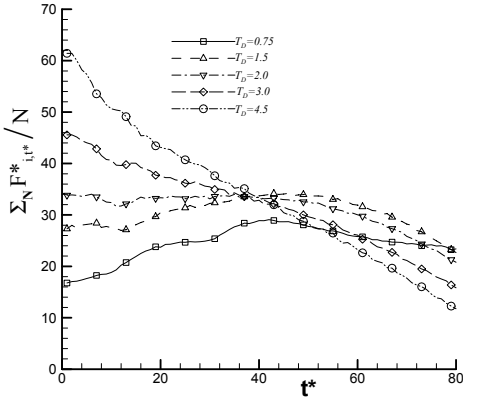

Figure 12: Evolution of the averaged non-dimensionalized intermolecular force for different temperatures (cases 1∼5 in Table 1)

the liquid particles and has a great effect upon the vaporization process. Figure 12 shows the evolution of averaged non-dimensionalized intermolecular force for nanojets with different temperatures (cases 1∼5 in Table 1) and the conditions of $L^*_2 = L^*_3 = L^*_4$=5.73, L^*_5=76.7, $D^*/2$=8.81. The averaged non-dimensionalized intermolecular force at time t^* is defined as

$$\overline{F^*_{t^*}} = \frac{\sum_{i=1}^{N} F^*_{i,t^*}}{N} \tag{5}$$

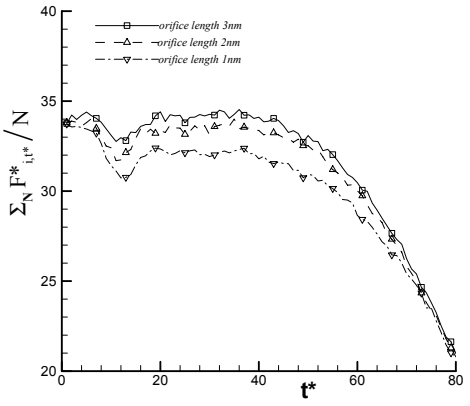

Figure 13: Evolution of the averaged non-dimensionalized intermolecular force for different orifice lengths (cases 3, 6 and 7 in Table 1)

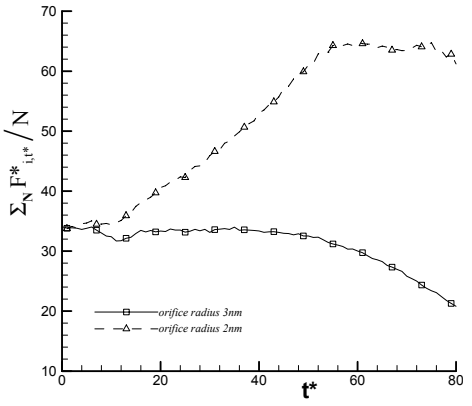

Figure 14: Evolution of the averaged non-dimensionalized intermolecular force for different orifice radii (cases 3 and 8 in Table 1)

where N is the total number of molecules in the fundamental cell and F^*_{i,t^*} is the resultant force of the non-dimensionalized intermolecular force vector acting on molecule i at time t^* , i.e. $F^*_{i,t^*} = ({F^*_{x,i,t^*}}^2 + {F^*_{y,i,t^*}}^2 + {F^*_{z,i,t^*}}^2)^{1/2}$, where F^*_{x,i,t^*}, F^*_{y,i,t^*} and F^*_{z,i,t^*} are the components of the intermolecular force vector at the x, y and z directions, respectively, acting on molecule i at time t^*. Note that in the above definition of $\overline{F^*_{t^*}}$, N is the total number of molecules in the fundamental cell, which includes liquid, vapor and solid molecules (nozzle and push panel); while in the definition of density uniformity factor, Eq.(4), N is the initial number of liquid molecules in the fundamental cell, while the solid molecules are excluded. The intermolecular force diminishes with time because of the increase of distances between molecules as the nanojet vaporizes. From Fig.12, it is observed that a higher temperature nanojet evaporates faster than a lower temperature one. This corroborates the results of Figs.3$\sim$7 discussed in section 3.1 and Fig.9 in section 3.2. In Fig.12, it is also noted that although a higher temperature nanojet has a larger intermolecular force at the earlier stage of the vaporization process due to its higher momentum, it evaporates faster and therefore the intermolecular force decays quicker. Figure 13 shows the time averaged value of the averaged non-dimensionalized intermolecular force for different orifice lengths (cases 3, 6 and 7 in Table 1) on the basis of identical nozzle orifice diameter (6 nm) and the conditions of L^*_3=5.73, L^*_5=76.7, T^*=2.0. It is observed that a nanojet with a shorter orifice length evaporates quicker. This corroborates the results of Figs.8(a), (b) and (c) as discussed in section 3.1 and Fig.10 as discussed in section 3.2. Figure 14 shows the evolution of density uniformity factor for different orifice diameters (cases 3 and 8 in Table 1)

on the basis of identical nozzle orifice length (2 nm) and the conditions of L_4^*=5.73, L_5^*=76.7, T^*=2.0. It is observed that a nanojet with a larger orifice diameter evaporates quicker. This corroborates the results of Figs.8(a) and (d) and also reveals that a nanojet from a nozzle with a smaller orifice length/diameter ratio moves farther due to its smaller frictional loss.

Conclusions

In this study, the vaporization process of a nanojet is investigated by molecular dynamics simulation. It is found that a liquid nanojet evaporates faster at higher temperatures. On the basis of identical nozzle orifice diameter, a nanojet from a nozzle with a shorter orifice length evaporates quicker. On the other hand, on the basis of identical nozzle orifice length, a nanojet from a nozzle with a larger orifice diameter evaporates quicker. The present simulation results can provide insight into the fundamental mechanism of the atomization process and will be helpful for the design of nanojet devices such as nano-printer or nano-sprayer.

Acknowledgement

The author gratefully acknowledges the grant support from the National Science Council, R.O.C., under the contract NSC97-2221-E-150-029.

References

1. C. L. Yeh, Turbulent Flow Investigation inside and outside Plain-Orifice Atomizers with Rounded Orifice Inlets, Heat and Mass Transfer 41 (9) (2005) 810-823.
2. C. L. Yeh, Analysis of the Vaporization Process for a Nano-Scale Liquid Thread by Molecular Dynamics Simulation, accepted for publication in International Journal of Heat and Mass Transfer.
3. Lord Rayleigh, On the Stability of Jets, Proceedings of the London Mathematical Society 10, 1879, pp.4-13.
4. J. Koplik, J. R. Banavar, Molecular Dynamics of Interface Rupture, Physics of Fluids A 5 (3) (1993) 521-536.
5. S. Kawano, Molecular Dynamics of Rupture Phenomena in a Liquid Thread, Physical Review E 58 (4) (1998) 4468-4472.
6. M. Moseler and U. Landman, "Formation, Stability, and Breakup of Nanojets," *Science*, Vol.289, pp.1165-1169, 2000.
7. H. Shin, M. Oschwald, M. M. Micci and W. Yoon, "Influence of Thermodynamic State on Nanojet Break-up", *Nanotechnology*, Vol.16, pp.2838–2845, 2005.
8. Yong Seok Choi, Sung Jin Kim, and Moon-Uhn Kim, "Molecular Dynamics

of Unstable Motions and Capillary Instability in Liquid Nanojets", Physical Review, E, Vol.73, 016309, 2006.

9. J. M. Haile, Molecular Dynamics Simulation, John Wiley & Sons, New York, 1992, chap.5.
10. A. H. Lefebvre, Atomization and Sprays, Hemisphere, New York, 1989, chap.2.